Science Advances

AAAS

advances.sciencemag.org/cgi/content/full/2/6/e1600477/DC1

Supplementary Materials for

Tunable room-temperature spin-selective optical Stark effect in solution-processed layered halide perovskites

David Giovanni, Wee Kiang Chong, Herlina Arianita Dewi, Krishnamoorthy Thirumal, Ishita Neogi, Ramamoorthy Ramesh, Subodh Mhaisalkar, Nripan Mathews, Tze Chien Sum

Published 17 June 2016, *Sci. Adv.* **2**, e1600477 (2016)
DOI: 10.1126/sciadv.1600477

The PDF file includes:

- table S1. Comparison of OSE and Rabi energy in various inorganic semiconductors.
- References (*28*–*36*)

A. Experimental Setup

The laser system used is the 800 nm Coherent Inc. Libra^{TM} Ti:Sapphire laser with ~50 fs pulse width at a 1 kHz repetition rate. The output was split into two beams. One beam was directed to the optical parametric amplifier (Coherent OPerA SOLO^{TM}) to generate tunable photon energy for the pump. The weaker beam was steered to a delay stage before being focused to a sapphire crystal for white light generation (1.4 eV – 2.8 eV), as shown in the Transient Absorption (TA) setup in fig. S1 below. The measurement was performed in transmission mode. Transmitted probe was collected and sent to monochromator and photo multiplier tube (PMT) with lock-in detection (at a chopper frequency of 83 Hz). Linear polarizers were used for both the linearly polarized pump and probe measurements. A Solei Babinet Compensator (SBC) and an achromatic quarter wave plate (λ/4) were used to generate circular polarization for the pump and probe beams, respectively for the circularly pump and probe measurements. Intensity control in this experiment was performed by using variable density filters. Chirp-correction in the TA spectra was also implemented.

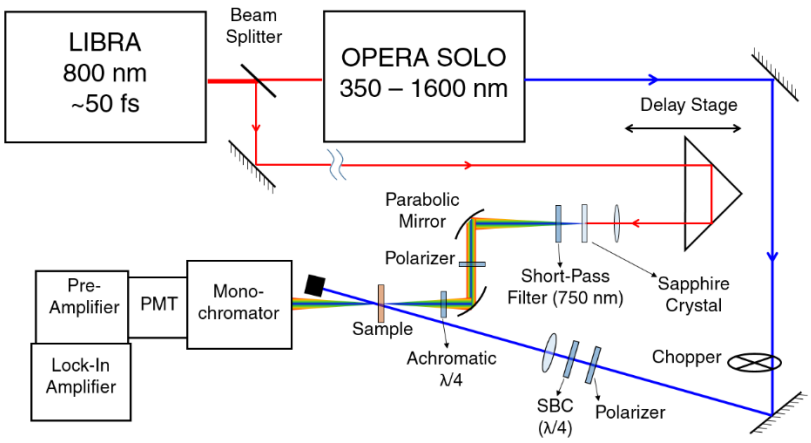

fig. S1. TA spectroscopy setup. The schematic of our femtosecond TA spectroscopy setup used in this work for circularly pump and probe measurements. For the linearly pump and probe measurements, the SBC and the achromatic λ/4 waveplate were replaced with linear polarizers.

B. Estimation of Energy Shift Δ*E*

For a given spectrum described by function *f*(*x*), we can calculate the transient change of the spectrum due to a positive shift of Δ*x*. The transient change Δ*f*, as illustrated by fig. S2, can be described as

$$\Delta f(x) = f(x-\Delta x) - f(x) \approx -\frac{df(x)}{dx}\Delta x \qquad \text{(S1)}$$

which is proportional to the first derivative of the function. For a known *f*(*x*), the first derivative can be analytically solved and used to fit the experimental data to estimate Δ*x*. Nevertheless, for a general case of an unknown peak function *f*(*x*), another approach to estimate Δ*x* would be through what is defined as spectral weight transfer (SWT)

$$\mathrm{SWT} = \int_0^{x_0} \Delta f(x)dx \qquad \text{(S2)}$$

where x_0 is the peak position. SWT can be easily calculated numerically from our experimental data, without knowing the analytical function.

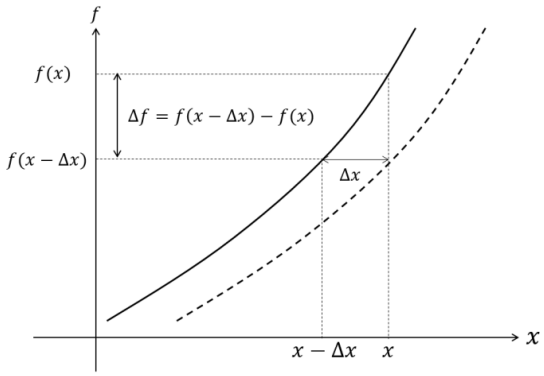

fig. S2. Calculation of transient change due to positive *x* shift. When the function *f*(*x*) is shifted in positive *x*-direction by Δ*x*, the transient change at *x* due to the shift is given by Δ*f*(*x*) = *f*(*x* – Δ*x*) – *f*(*x*).

By the first fundamental theorem of calculus, eq. (S1) substituted to eq. (S2), can be simplified into

$$\mathrm{SWT} = -\Delta x \int_0^{x_0} \frac{df(x)}{dx} dx = -\Delta x (f(x_0) - f(0)) \tag{S3}$$

For our case, $f(x)$ is $A(E)$, where $A(E)$ is the absorbance of the material as a function of photon energy E. Since we have $A(0) = 0$, the energy shift ΔE due to the optical Stark effect (with E_0 is the peak absorption energy) in our experiment can be estimated as

$$\Delta E = -\frac{\mathrm{SWT}}{A(E_0)} = -\frac{1}{A(E_0)} \int_0^{E_0} \Delta A(E) \mathrm{d}E \tag{S4}$$

Here, $A(E_0) = 1.186$ OD at $E_0 = 2.39$ eV which is the peak absorbance (main text – Fig. 1C). As the OSE signal vanishes below 2.25 eV, the integration limits are set within range 2.25 eV ≤ E ≤ 2.39 eV.

C. Quantum Mechanical Description of the Optical Stark Effect (OSE)

We start by applying the Jaynes-Cummings model of interaction in a system with two optically coupled eigenstates $|1\rangle$ and $|2\rangle$ with energy E_1 and E_2, respectively, i.e., $E_2 - E_1 = \hbar\omega_0 > 0$, in the presence of electromagnetic radiation with photon energy $\hbar\omega$. The total Hamiltonian of the system comprises of three distinct components

$$H_S = E_1 |1\rangle\langle 1| + E_2 |2\rangle\langle 2| \tag{S5}$$

$$H_L = \hbar\omega \left(\hat{a}^\dagger \hat{a} + \frac{1}{2} \right) \tag{S6}$$

$$H_I = \hbar\omega_R \left(|1\rangle\langle 2| \hat{a}^\dagger + |2\rangle\langle 1| \hat{a} \right) \tag{S7}$$

where H_S, H_L and H_I are the Hamiltonian of the two-level system, the electromagnetic (EM) radiation, and the interaction between them, respectively. The *Rabi frequency* is given by

$\Omega_R = 2\omega_R\sqrt{(n+1)}$, where ω_R is the *vacuum Rabi frequency* and n is the number of photons in the system. The vacuum Rabi frequency ω_R is given by

$$\omega_R = |p_{12}|\sqrt{\frac{\hbar\omega}{2\epsilon V_m}} \tag{S8}$$

The $|p_{12}| = \langle 1|p|2\rangle$ is the transition dipole moment which contains the optical selection rule for transition, where p is the electric dipole operator, ϵ is the dielectric constant and V_m is the photon confinement (cavity mode) volume (*28*, *29*). The inverse relation between the Rabi frequency to the square root of the photon confinement volume allows for additional degree of freedom to tune Ω_R using different cavities. In our case, no external photonic cavity is used in our spin-coated thin films.

Here, Ω_R parameterizes the coupling strength between the system and the EM radiation. The operators $\hat{a}^\dagger$ and $\hat{a}$ are the creation and annihilation operators of the photon, respectively, which act on the Fock states $|n\rangle$ as follows

$$\hat{a}^\dagger|n\rangle = \sqrt{n+1}|n+1\rangle \tag{S9}$$

$$\hat{a}|n\rangle = \sqrt{n}|n-1\rangle \tag{S10}$$

The total Hamiltonian of the system is given by the summation of H_S, H_L and H_I. Here, the two states that we are interested are: $|1,n+1\rangle$ and $|2,n\rangle$. Using these two states $\{|1,n+1\rangle,|2,n\rangle\}$ as the basis, the total Hamiltonian can be written in matrix representation as

$$H = \begin{pmatrix} E_1 + \hbar\omega\left(n+\frac{3}{2}\right) & \frac{1}{2}\hbar\Omega_R \\ \frac{1}{2}\hbar\Omega_R & E_2 + \hbar\omega\left(n+\frac{1}{2}\right) \end{pmatrix} \tag{S11}$$

Without the loss of generality, we can set the energy level reference such that $E_1 = -\hbar\omega_0/2$ and $E_2 = \hbar\omega_0/2$. The Hamiltonian can therefore be rewritten as

$$\begin{aligned} H &= \begin{pmatrix} -\frac{\hbar\omega_0}{2} + \hbar\omega\left(n+\frac{3}{2}\right) & \frac{1}{2}\hbar\Omega_R \\ \frac{1}{2}\hbar\Omega_R & \frac{\hbar\omega_0}{2} + \hbar\omega\left(n+\frac{1}{2}\right) \end{pmatrix} \\ &= \begin{pmatrix} -\frac{\Delta}{2} + \hbar\omega(n+1) & \frac{1}{2}\hbar\Omega_R \\ \frac{1}{2}\hbar\Omega_R & \frac{\Delta}{2} + \hbar\omega(n+1) \end{pmatrix} \end{aligned} \tag{S12}$$

where $\Delta = \hbar\omega_0 - \hbar\omega$ is the detuning energy between the equilibrium state and the photon energy of the laser. If the two-states are not optically coupled, *i.e.*, $\Omega_R = 0$, the Hamiltonian will reduce to

$$H = \begin{pmatrix} -\frac{\Delta}{2} + \hbar\omega(n+1) & 0 \\ 0 & \frac{\Delta}{2} + \hbar\omega(n+1) \end{pmatrix} \tag{S13}$$

In this case for the Hamiltonian without light-matter interaction in eq. (S13), the eigenstates of $|1, n+1\rangle$ and $|2, n\rangle$ are called bare states.

In the presence of light-matter interaction, $\Omega_R > 0$. $|1, n+1\rangle$ and $|2, n\rangle$ are no longer the eigenstates of the system, as the Hamiltonian is not diagonal. The new eigenstates can be obtained by diagonalizing the Hamiltonian in eq. (S12)

$$H = \hbar\omega(n+1)\begin{pmatrix} 1 & 0 \\ 0 & 1 \end{pmatrix} + \begin{pmatrix} -\frac{1}{2}\sqrt{(\hbar\Omega_R)^2 + \Delta^2} & 0 \\ 0 & \frac{1}{2}\sqrt{(\hbar\Omega_R)^2 + \Delta^2} \end{pmatrix} \tag{S14}$$

with two new eigenstates $|n-\rangle$ and $|n+\rangle$ as the new basis of the diagonalized Hamiltonian. The constant energy shift of $\hbar\omega(n + 1)$ in the eigenenergies is due to the presence of other photons in the system. Here, $\sqrt{(\hbar\Omega_R)^2 + \Delta^2}/\hbar$ is also called as *generalized Rabi frequency*. The relation between the new basis set and the previous basis set are given by

$$|n-\rangle = -\sin\theta_n |1, n+1\rangle + \cos\theta_n |2, n\rangle \tag{S15}$$

$$|n+\rangle = \cos\theta_n |1, n+1\rangle + \sin\theta_n |2, n\rangle \tag{S16}$$

$$\cos\theta_n = \frac{\sqrt{(\hbar\Omega_R)^2 + \Delta^2} - \Delta}{\sqrt{\left(\sqrt{(\hbar\Omega_R)^2 + \Delta^2} - \Delta\right)^2 + (\hbar\Omega_R)^2}} \tag{S17}$$

$$\sin\theta_n = \frac{\hbar\Omega_R}{\sqrt{\left(\sqrt{(\hbar\Omega_R)^2 + \Delta^2} - \Delta\right)^2 + (\hbar\Omega_R)^2}} \tag{S18}$$

These two new eigenstates are also known as the *Floquet states* or dressed states, which are also known as *exciton-polariton* states in the case for semiconductors. A plot of the eigenenergies as function of $\hbar\omega$ for the case of with (solid lines) and without light-matter interaction (dashed lines) is given in fig. S3A. As expected, the two eigenenergies of the bare states are degenerate for the case of resonant photon energy ($\Delta = 0$); the energy of n photon with the system in the excited state $|2\rangle$ is equal to energy of $n + 1$ photon with the system in the ground state $|1\rangle$. An important phenomenon shown in the figure is that the energy gap between the two new eigenstates $|n+\rangle$ and $|n-\rangle$ (upper and lower polariton branch, respectively) is increased by the interaction with the photon, as compared to the

gap between the bare states ($|2,\ n\rangle$, $|1,\ n+1\rangle$). This is known as the *AC Stark effect* or *Optical Stark Effect* (OSE). OSE causes the absorption spectrum of the system to shift by ΔE, which is related to the *Rabi energy* ($\hbar\Omega_R$) and detuning energy Δ as

$$\Delta E = \sqrt{(\hbar\Omega_R)^2 + \Delta^2} - \Delta \approx \frac{(\hbar\Omega_R)^2}{2\Delta} \propto \text{ Intensity} \tag{S19}$$

The approximation is valid for the case of $\Delta >> \hbar\Omega_R$. Since Ω_R is proportional to the electric field induced by light, the Stark shift is therefore expected to be linear to the pump fluence.

Figure S3B plots the dispersion relation (energy vs momentum) of the dressed states (solid lines) and the bare states (dashed lines), for the case of the exciton in a semiconductor. The dispersion relation of a bare exciton E_X and a bare photon E_{ph} are given by

$$E_X = \hbar\omega_0 + \frac{p^2}{2M} \tag{S20}$$

$$E_{ph} = \frac{c}{n}p \tag{S21}$$

where p is the momentum, M is the exciton mass and n is the refractive index. Note that this equation applies in the approximation of $\hbar\omega_0 >> p^2/2M$, such that the resonance ($\Delta = 0$) occurs at $E_{ph} \approx \hbar\omega_0$. The dispersion relation of the polariton, which is a photon-dressed state of exciton (or a quasi-particle hybrid of the photon and exciton), is therefore given by

$$\begin{aligned} E &= \frac{E_X + E_{ph}}{2} \pm \frac{1}{2}\sqrt{(\hbar\Omega_R)^2 + \Delta^2} \\ &= \frac{1}{2}\left(\hbar\omega_0 + \frac{p^2}{2M} + \frac{c}{n}p\right) \pm \frac{1}{2}\sqrt{(\hbar\Omega_R)^2 + (\hbar\omega_0 - \frac{c}{n}p)^2} \end{aligned} \tag{S22}$$

The + and – signs are for upper and lower polariton branches, respectively. It is clear from such relation that when there is no interaction (*i.e.*, $\Omega_R = 0$), the energy dispersion will

reduce to either the bare exciton or bare photon case with a crossing between them at resonance. The gap of the anti-crossing for the case of $\Omega_R > 0$ at resonance is called the Rabi energy.

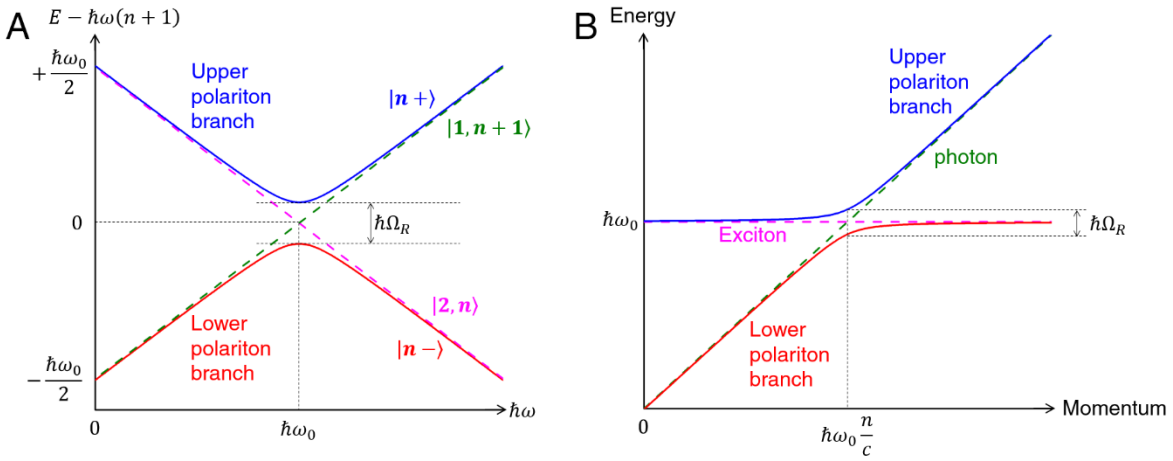

fig. S3. Quantum description of OSE. (A) A schematic of the new eigenenergies of the photon-dressed states (solid line) in relation to the bare states (dashed line). The Optical Stark Effect (OSE) gives rise to the separation between the two eigenenergies in the dressed states as compared to the bare states. **(B)** Dispersion relation for the two new photon-dressed eigenstates for the case of the exciton in a semiconductor.

D. Estimation of the Rabi Energy

From eq. (S18) and our experimental values for Δ = 0.23 eV and ΔE = 4.5 ± 0.2 meV, we estimate the Rabi energy of our PEPI thin film system at the fluence of 1.66 mJ/cm^2 to be $\hbar\Omega_R$ = 47 ± 2 meV.

As a self-consistency check on the model, we also repeated the experiments with a different detuning energy Δ = 0.33 eV. The results are plotted in fig. S4, which also show a linear relationship. Since Ω_R is proportional to the electric field of the light, *i.e.*, the square root of the number of photons or the square root of the intensity (fluence divided by pulse width), we estimate the Ω_R for the case Δ = 0.33 eV at a fluence 1.46 mJ/cm^2 to be

$$\hbar\Omega_R \approx 47\ \text{meV} \times \sqrt{\frac{1.46\ \text{mJ/cm}^2}{1.66\ \text{mJ/cm}^2} \times \frac{290\ \text{fs}}{680\ \text{fs}}} \approx 29\ \text{meV} \tag{S23}$$

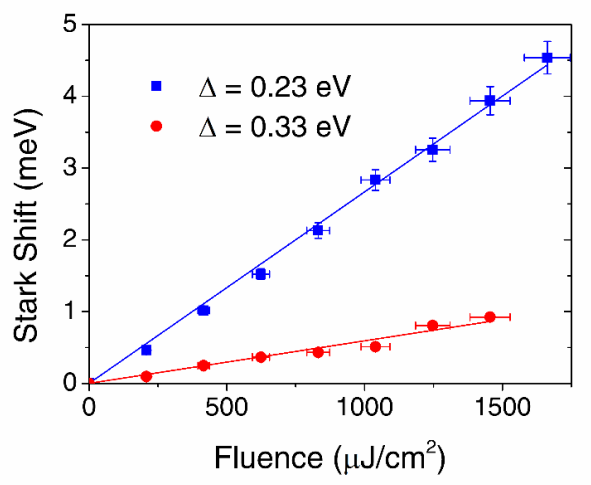

fig. S4. OSE with different pump detuning. Calculated spectral weight transfer (SWT) and estimated Δ*E* due to OSE for pump detuning Δ = 0.23 eV (black, pump at 2.16 eV) and Δ = 0.33 eV (red, pump at 2.07 eV).

Here, we also have to take into account the effect of the difference in the pump pulse durations, which we obtained from the pump-probe cross correlation in our setup – see fig. S5B. Using this value of Rabi frequency $\hbar\Omega_R$ = 29 meV, the OSE energy shift at Δ = 0.33 eV and fluence 1.46 mJ/cm^2, the energy shift Δ*E* can be estimated to be Δ*E* ≈ 1.2 meV, which is consistent with our obtained experimental value of 0.92 ± 0.05 meV, as shown in fig. S4.

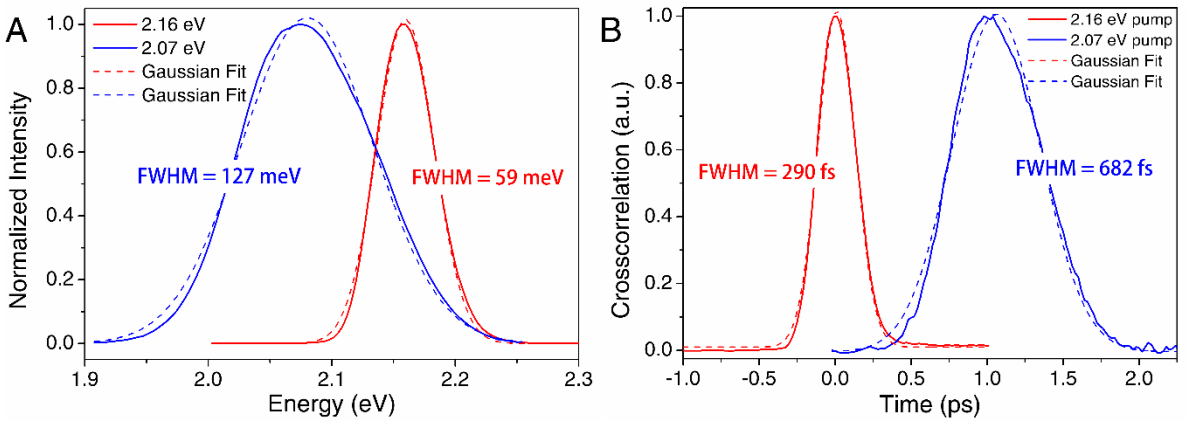

fig. S5. Pump properties in the energy and time domains. (A) Pump spectra for 2.16 eV (red) and 2.07 eV (blue) used in our experiment with the FWHM values shown. **(B)** Pump-probe cross-correlation obtained with 2.37 eV probe, for 2.16 eV (red) and 2.07 eV (blue) with the FWHM values offset in the time axis for clarity.

E. Comparison of Rabi Energy

Comparison of energy shift by OSE and the value of Rabi energy for various inorganic semiconductor is presented in the table S1, together with the laser system and intensity reported to reach such energy. A fair comparison can only be made on GaAs/AlGaAs quantum well, due to similar femtosecond laser system and pump intensity; in which PEPI thin films prevails by ~4 times higher magnitude of Rabi energy. Moreover, such value is reached in room temperature, as contrast to cryogenic temperature typically used for study in inorganic semiconductor nanostructures.

table S1. Comparison of OSE and Rabi energy in various inorganic semiconductor. Compilation of various OSE and Rabi energy in semiconductor nanostructures reported in the literature. The information of laser system and intensity/power used to obtain such energy is also included. Abbreviation of MQW, QD and CW refer to multiple quantum well, quantum dot and continuous wave, respectively.

Material	Pump Intensity (Laser System)	T (K)	Δ (meV)	ΔE (meV)	$\hbar\Omega_R$† (meV)
PEPB thin film (our result)	5.5 GW/cm^2	300	460	1.2	33
PEPI thin film (our result)	5.5 GW/cm^2	300	230	4.5	47
FPEPI thin film (our result)	5.5 GW/cm^2	300	230	6.3	55
Single Mn-doped CdTe QD (10-20 nm). (*4*)	Power not stated (CW single-mode dye ring laser)	5	0	0.25	0.25
9.6 nm GaAs/9.8 nm $A1_{0.27}Ga_{0.73}As$ MQW. (*30*)	8 MW/cm^2 (6-ps 6.7-MHz mode-locked cavity dumped dye laser)	70	18	0.1	1.9
10 nm GaAs/10 nm AlGaAs MQW. (*27*)	~10 GW/cm^2 (150-fs colliding-pulse mode-locked laser.)	15	29	~1.4*	9.1
10 nm GaAs/2.5 nm AlGaAs MQW. (*27*)	~10 GW/cm^2 (150-fs colliding-pulse mode-locked laser.)	15	19	~3.5#	12
Single InAs QD (50 nm) in GaAs photonic crystal. (*31*)	60 μW (CW 300-kHz-FWHM λ-tunable laser diode)	14	0.43	0.083	0.28
Single Interface QD (50 nm) in GaAs/AlAs superlattice (*5*)	0.2 μW (2-ps 0.8-meV-FWHM Ti:S oscillator + fiber)	12	3	~0.47	1.75

* Estimated energy shift from Fig. 1 in Ref. (*27*)
# Estimated energy shift from Fig. 2 in Ref. (*27*)
† The value is estimated from eq. (S19), if not directly mentioned.

F. Estimation of the Equivalent B-field for Zeeman Splitting of Energy Levels

The energy level E for a system in a magnetic field B is given by

$$E = E_0 \pm \frac{1}{2} g_J \mu_B m_J B + c_0 B^2 \quad \text{(S24)}$$

Here, E_0 is the energy level in the absence of a B-field, g_J is the effective g-factor, m_J is the projection of total angular momentum quantum number in z direction (*i.e.,* B-field direction), μ_B = 57.88 μeV/T is the Bohr magneton and c_0 is the diamagnetic coefficient. The + and – signs refer to states with the magnetic moment anti-parallel and parallel to the B-field, respectively. For a system with m_J = ±1/2, the splitting of the spin-state gives rise to

$$\Delta E = E_+ - E_- = g_J \mu_B B \quad \text{(S25)}$$

where E_+ and E_- correspond to the absorption of σ^+ and σ^-, respectively.

However, to the best of our knowledge, there are no reports in literature on the measurement of spin-state splitting by B-field for PEPI (*i.e.* Zeeman Effect) nor its *g*-factor. Considering that the organic component only gives a weak contribution [see (*22*)] we proceed to estimate the equivalent B-field for the OSE splitting in PEPI using the *g* values measured for a similar perovskite that has a different organic component $(C_{10}H_{21}NH_3)_2PbI_4$. There is a range of values reported for the *g*-factor of $(C_{10}H_{21}NH_3)_2PbI_4$. Xu *et al.* reported *g*-factors of 0.77 to 1.08 in (*32*). Using these values, we obtained an equivalent B-field of ~71 T to ~99 T (or ~99 T to 140 T) for the 4.5 meV (or 6.3 meV) energy splitting. On the other hand, Hirasawa *et al*. reported a value of 1.42 (*33*), which would yield an estimated equivalent B-field of ~54 T (or ~76 T for FPEPI) for the 4.5 meV (or 6.3 meV for FPEPI) splitting. Hence, we conservatively estimate that that our OSE-induced spin-state splitting in PEPI is equivalent with a Zeeman splitting with B-field of >50 Tesla (or >70 T for FPEPI).

G. Estimation of the Transition Dipole Moment (TDM) of PEPI

From our results, we can also estimate the exciton transition dipole moment (TDM) of PEPI. The electric field *F* due to our pump pulse of 1.66 mJ/cm^2 (at 2.16 eV) can be estimated using the relation with the peak intensity *I*

$$I = \frac{\text{fluence}}{\text{duration}} = \frac{1}{2} n \epsilon_0 c F^2 \tag{S26}$$

where $n \approx 2.1 \pm 0.1$ ($n \approx 2.0 \pm 0.1$) is the refractive index of PEPI (PEPB) film at pump energy – see (*14*, *20*, *34*). From this relation we obtain $F = 143 \pm 4$ MV/m with pulse duration of 290 fs – Fig. S5B ($F = 101 \pm 5$ MV/m for PEPB). From semi-classical quantum theory, the Rabi frequency of a system is related to the electric field *F* of the EM radiation through

$$\hbar\Omega_R = |p_{12}| F \propto \sqrt{\text{Intensity}} \tag{S27}$$

Given $\hbar\Omega_R = 47 \pm 2$ meV for PEPI ($\hbar\Omega_R = 33 \pm 3$ meV for PEPB – see Supplementary Material Section H), the transition dipole moment is determined to be $|p_{12}| = (5.26 \pm 0.20) \times 10^{-29}$ C m = 15.8 ± 0.6 Debye ($|p_{12}| = (5.16 \pm 0.50) \times 10^{-29}$ C m = 15.5 ± 0.6 Debye for PEPB).

H. Estimation of $\hbar\Omega_R$ and Oscillator Strength in Various Organic-Inorganic Halide Perovskite systems

Figure S6 shows comparison of three halide perovskite system with varying dielectric contrast between the barrier and the well layers, from the lowest to highest: PEPB, PEPI and FPEPI – fig. S6A. Figure S6B and C shows a linear and square-root dependence of observed Stark shift and Rabi energy to the pump fluence, which is in accordance to eq. (S19) and eq. (S27), respectively. Higher Rabi energy is achieved by halide perovskite system with larger dielectric contrast, which implies it as the determining parameter for light-matter coupling strength in this material system. At fluence of 1.66 mJ/cm^2, we achieve ΔE of 1.2 ± 0.1 meV (at Δ = 0.46 eV), 4.5 ± 0.2 meV (at Δ = 0.23 eV) and 6.3 ± 0.3 meV (at Δ = 0.23 eV) for PEPB, PEPI and FPEPI, respectively. These values correspond to respective Rabi energy $\hbar\Omega_R$ of 33 ± 3 meV, 47 ± 2 meV and 55 ± 2 meV. Meanwhile, it is known that the oscillator strength *f* of a transition is proportional to the integration of the absorption coefficient over the spectrum (eq. S28) (*35*)

$$f \propto \int_0^\infty \alpha(\omega) d\omega \tag{S28}$$

The oscillator strengths of these three materials are therefore estimated by integrating the area of Lorenztian function fitted to the free exciton peak – fig. S7C. Given the oscillator strength of PEPI to be ~0.5 (*14*) the oscillator strength for two other materials are scaled accordingly. We estimate the oscillator strength of PEPB to be ~0.99 (indicated by much stronger absorption), while the oscillator strength of FPEPI to be ~0.54 (similar to PEPI). Surprisingly PEPB, while having a lowest dielectric contrast and Rabi energy among them, it possesses the highest oscillator strength. Here, we demonstrated that oscillator strength is not the direct determining parameter for light-matter coupling strength, due to interplay of other various factors – eq. (S30).

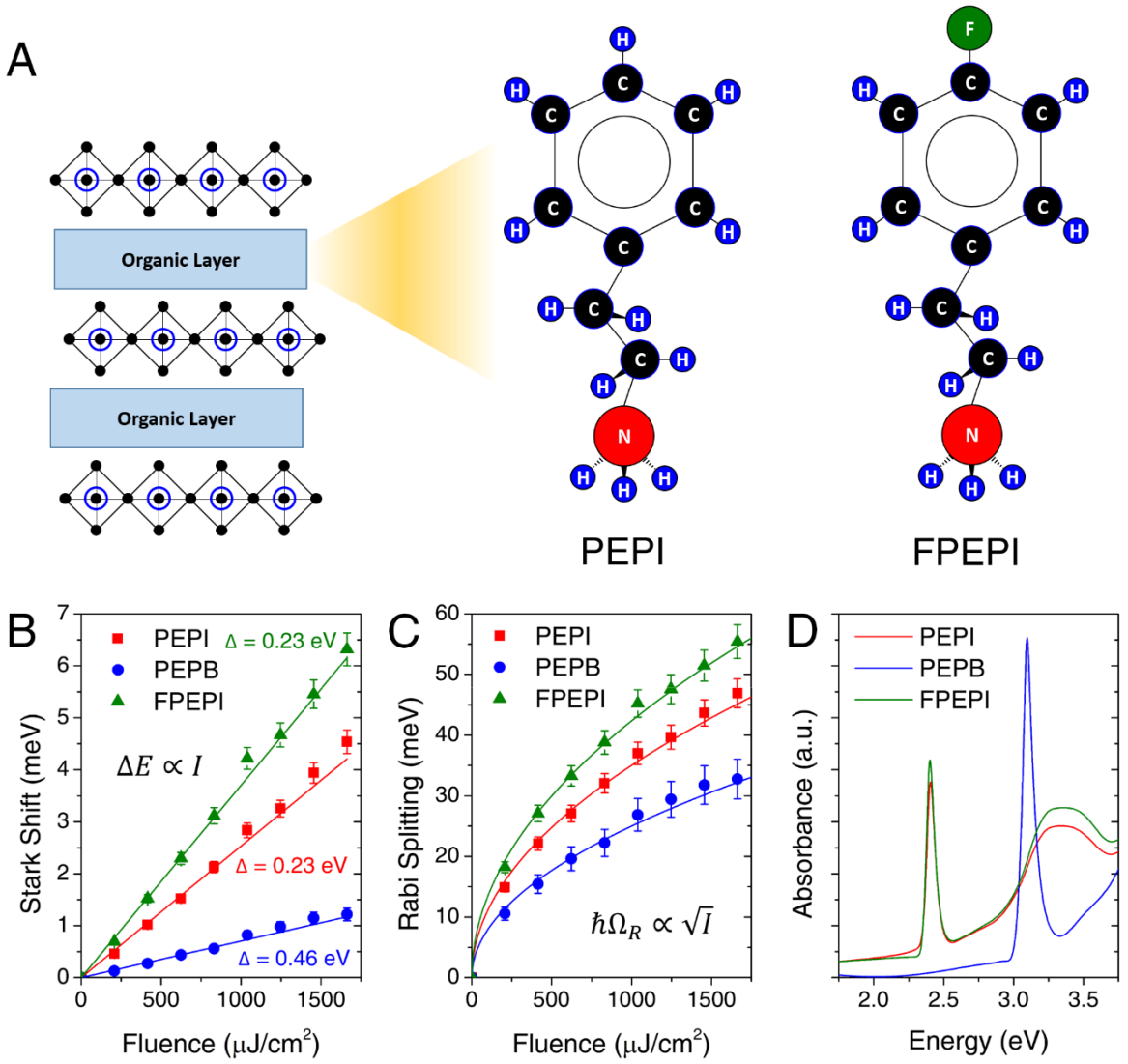

fig. S6. Comparison of various halide perovskite with different dielectric contrast. (A) Structural difference between organic component of PEPI and FPEPI. **(B)** The stark shift, **(C)** the Rabi energy as function of pump fluence and **(D)** the absorption spectrum of PEPI (red), PEPB (blue) and FPEPI (green). The dielectric contrast between the barrier and the well is increasing with the following order: PEPB, PEPI and FPEPI.

I. Estimation of the Exciton Reduced Mass

The relation between the transition dipole moment (TDM), oscillator strength *f* and effective mass *m** is given by (*35*)

$$f = \frac{2m^*\omega_{12}\left|p_{12}\right|^2}{3e^2\hbar} \tag{S29}$$

Here, ω_{12} is the transition frequency between states $|1\rangle$ and $|2\rangle$. Given the oscillator strength of *f* = ~0.5 for PEPI and *f* = ~0.99 for PEPB, the electron effective mass can be calculated to be $m^* = (0.22 \pm 0.01)m_0$ for PEPI and be $m^* = (0.35 \pm 0.03)m_0$ for PEPB; where $m_0 = 9.1 \times 10^{-31}$ kg is the rest mass of free electron. Assuming the effective mass of electron and hole $m_e^* = m_h^*$, which is common assumption for layered perovskite system (*36*), the exciton reduced mass is therefore given by $\mu = (0.11 \pm 0.01)m_0$ for PEPI and $\mu = (0.18 \pm 0.02)m_0$ for PEPB. This result is consistent with the report of $0.09m_0$ on PEPI by Hong *et al.* (*14*) and of $0.17m_0$ on PEPB by Tanaka *et al.* (*20*), which are estimated by using different experimental techniques. This result also validates our estimation of oscillator strength.

J. Estimation of the Radiative Lifetime

Using the obtained transition dipole moment (TDM), we estimate the radiative lifetime (spontaneous emission) of the system. The spontaneous emission rate or Einstein coefficient *A*, is related to the transition dipole moment through

$$\tau_R = A^{-1} = \left(\frac{n^3\omega_0^3\left|p_{12}\right|^2}{3\epsilon_0\pi\hbar c^3} \right)^{-1} \tag{S30}$$

Using the obtained $|p_{12}|$, we estimate the radiative lifetime to be 190 ± 10 ps. This value is consistent with our measurement of the time-resolved photoluminescence (PL) lifetime of 210 ± 10 ps, as shown in fig. S7. This further validates our estimation of $|p_{12}|$.

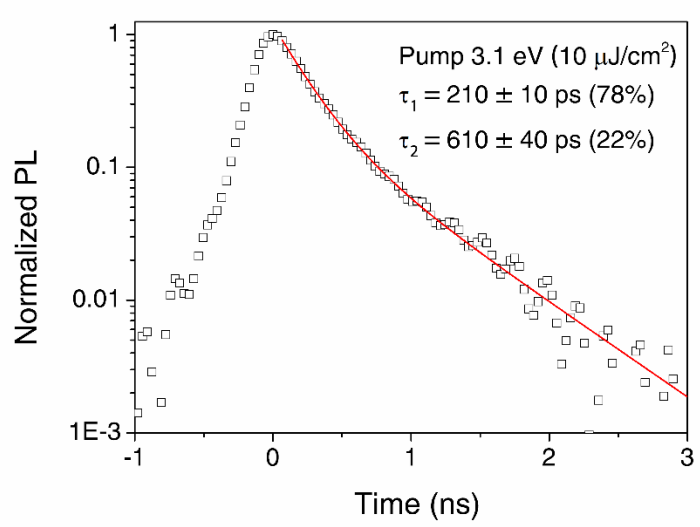

fig. S7. Photoluminescence kinetics of PEPI. The PL kinetics by 3.1 eV pump with fluence of 10 μJ/cm^2. The kinetics is fitted with two lifetimes, which yields a short component of 210 ± 10 ps (78%) and a long component of 610 ± 40 ps (22%). The short component is attributed to spontaneous emission from the free exciton, while the long lifetime component originates from the bound exciton due to the spectral overlap of the free exciton and bound exciton peaks.

K. Oscillatory Signal in PEPI

As shown in Fig. 2D (main text), the kinetics for pump energy of 2.16 eV, which is below exciton absorption peak at 2.39 eV, shows a strong OSE signal and a weak oscillatory PB signal. To determine the origin of the oscillatory signal we performed pump-probe measurement with above bandgap pump excitation of 3.10 eV (*i.e.*, high enough to allow direct excitation of the excitons) – fig. S8A. The data shows a similar oscillatory signal of ~1 THz frequency, which confirms our deduction that the oscillations originate from the two-photon photoexcited excitons. Further confirmation is shown by fig. S8B. The TA spectrum

with pump excitation above the band-gap (3.1 eV), taken at 1 ps pump-probe delay, long after pulse duration but before significant exciton relaxation processes happen, shows a similar feature with the TA spectrum with pump excitation below bandgap (2.16 eV) and counter-circular pump-probe polarization. This confirms that the observed TA signal by sub-bandgap excitation with counter-circular pump-probe polarization comes from the two-photon photoexcited excitons. The TA spectrum with pump excitation above bandgap shows no dependence on pump-probe polarization. Hirasawa *et al.* (*33*) observed a strong Raman signal from optical phonons at 6.3 meV (~1.5 THz) for a similar layered perovskite $(C_{10}H_{21}NH_3)_2PbI_4$. This oscillatory signal could be from exciton-phonon interactions. Further experiments are required for its verification.

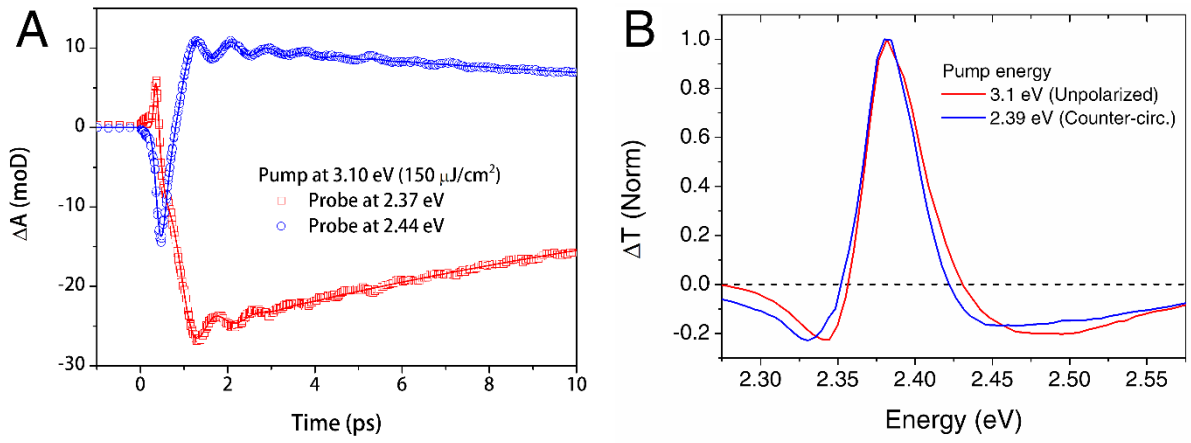

fig. S8. Exciton dynamics in PEPI. (A) The kinetics of 3.10 eV pump excitation, at 2.37 eV (red) and 2.44 eV (blue) probe, showing oscillatory signal with frequency of ~1 THz. **(B)** The comparison between TA spectra of by pump excitation above bandgap (3.10 eV) at 1 ps delay (red) and below bandgap (2.16 eV) at 0.4 ps delay (blue) with counter-circular pump-probe polarization. Pump excitation above band-gap exhibits polarization independency.

L. Effect of Pump Polarization Ellipticity

We also investigate the dependence on the ellipticity of the pump polarization. This can be done by simply changing the fast-axis orientation of the quarter-wave plate (λ/4) in the pump beam, and recording the OSE signal as function of its angle.

The signals at the specific pump polarizations: σ^+, linearly s-polarized (σ^S) and σ^-, with σ^+ probe are shown in fig. S9, A and B. As expected, the observed OSE effect by σ^+ probe depends only on the σ^+ component of the pump. When the pump polarization is linear, i.e., equal contributions from both σ^+ and σ^- components, the $-\Delta A$ signal is halved.

To further validate our hypothesis that σ^+ probe depends only on the σ^+ component of the pump, we performed OSE measurements at arbitrary pump ellipticity. Without the loss of generality, given the initial polarization (before λ/4) to be linearly s-polarized (θ = 0), the polarization state after passing through the λ/4 at angle θ, can be described by

$$|\psi\rangle = \cos\theta \begin{pmatrix} 1 \\ 0 \end{pmatrix} + e^{-i\pi/2} \sin\theta \begin{pmatrix} 0 \\ 1 \end{pmatrix} = \cos\theta \begin{pmatrix} 1 \\ 0 \end{pmatrix} - e^{i\pi/2} \sin\theta \begin{pmatrix} 0 \\ 1 \end{pmatrix} \tag{S31}$$

where $(1\ 0)^T$ and $(0\ 1)^T$ basis are the component projections to the fast and slow axis of the λ/4, respectively. Here, the component projected to the slow axis is phase-delayed by π/2. In this basis, the circular polarization state can be expressed as

$$|\sigma^+\rangle = \frac{1}{\sqrt{2}} \left[\begin{pmatrix} 1 \\ 0 \end{pmatrix} - e^{i\pi/2} \begin{pmatrix} 0 \\ 1 \end{pmatrix} \right] \tag{S32}$$

$$|\sigma^-\rangle = \frac{1}{\sqrt{2}} \left[\begin{pmatrix} 1 \\ 0 \end{pmatrix} + e^{i\pi/2} \begin{pmatrix} 0 \\ 1 \end{pmatrix} \right] \tag{S33}$$

The polarization state can therefore be expressed in the circular polarization basis

$$\begin{aligned}|\psi\rangle &= a|\sigma^{+}\rangle + b|\sigma^{-}\rangle \\ &= \frac{1}{\sqrt{2}}[\cos\theta + \sin\theta]|\sigma^{+}\rangle + \frac{1}{\sqrt{2}}[\cos\theta - \sin\theta]|\sigma^{-}\rangle\end{aligned} \tag{S34}$$

The σ^{+} component of the polarization state is therefore given by

$$|a|^2 = \frac{1}{2}(\cos\theta + \sin\theta)^2 = \frac{1}{2}(1 + \sin 2\theta) \tag{S35}$$

Eq. S35 is then used to fit the OSE maximum –ΔA signal (at 2.35 eV σ+ probe, Δt = 0 ps) as a function of the pump λ/4 angle – fig. S9C. A non-zero offset is added to the fitting, due to the two-photon absorption, which was discussed previously. The excellent agreement between eq. S35 and our experimental data validates our hypothesis.

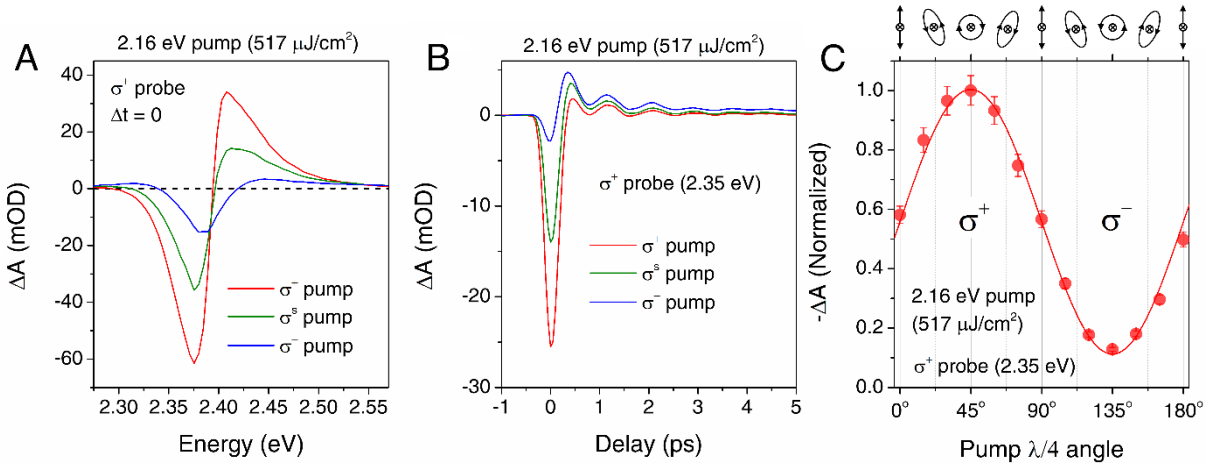

fig. S9. Polarization ellipticity control experiment of OSE in PEPI. (A) OSE spectrum at Δt = 0 ps and (B) Kinetics at 2.35 eV probe, in PEPI by using 2.16 eV pump (517 μJ/cm², Δ = 0.23 eV) at with σ^{+} (red), linearly s-polarized (σ^{S}, green) and σ^{-} (blue) pump polarization and σ^{+} probe polarization. Maximum normalized –ΔA signal (Δt = 0 ps) with 2.35 eV σ^{+} probe, as a function of pump ellipticity.